Electron impact dissociative ionization of ethane: Cross sections, appearance potentials, and dissociation pathways

Cechan Tian and C. R. Vidal
Max-Planck-Institut für Extraterrestrische Physik, P.O. Box 1603, 85740 Garching, Germany

(Received 22 December 1997; accepted 22 April 1998)

Cross sections of the electron impact ionization as well as the dissociative ionizations of ethane have been measured for electron energies from threshold to 600 eV. The complete collection of all the ionic fragments has been verified directly in the experiment. The results are thus believed to be reliable. The results for the products of $H_n^+(n=1-3)$ are obtained for the first time. The appearance potentials of the ionic products are also measured. The disagreement with respect to the appearance potentials between the present work and previous measurements is explained by the dipole-forbidden transitions in the electron impact excitation process. The starting channels for the ionic products are discussed based on the appearance potentials, the kinetic energy distributions of the ionic products, and the ejection of the electrons out of the different orbitals of the ethane molecule. © *1998 American Institute of Physics.* [S0021-9606(98)02129-1]

I. INTRODUCTION

Electron impact ionization and dissociative ionizations of ethane (C_2H_6) are of interest because of the existence of the molecule in the atmospheres of the outer planets and in plasma processing. For understanding the behaviors of ethane in different environments and the molecule itself, different efforts have been made to study the electronic structure, the ionization and the dissociative ionization of ethane, which includes the calculation of the electronic states of the ethane cation,[1–3] the $(e,2e)$ spectroscopy,[4] the study of the dissociation channels,[5,6] the measurements of the cross sections of photo- as well as electron impact ionization and dissociative ionizations.[6–9] However, so far only very little is known about the dynamics of the dissociative pathways. The existing cross section data are either inconsistent or incomplete.

In this paper we report the measurements of the cross sections of the electron impact dissociative ionization and the study of the dissociation pathways of ethane. The total cross section of electron impact ionization and dissociative ionization of ethane has been reported by Schram *et al.* for electron energy from 0.6 to 12 keV,[10] by Catham *et al.* from threshold to 300 eV,[8] by Durić *et al.* from threshold to 12 keV,[11] and by Nishimura and Tawara from threshold to 3 keV.[12] For the partial cross sections the only existing data are from Catham *et al.*[8] and Grill *et al.*[9] The two sets of data show very poor agreement with each other. Furthermore, the data are limited to the fragments of $C_2H_n^+(n=0-6)$ and $CH_n^+(n=0-3)$. No data on the fragments of $H_n^+(n=1-3)$ have ever been reported. We have made the cross section measurements for a complete set of singly charged fragments at electron energies from threshold to 600 eV. The appearance potentials, the kinetic energy distributions of the fragments near threshold are also measured to understand the starting channels of the dissociative ionizations of ethane.

II. EXPERIMENT

The experimental setup has been described in detail in previous papers.[13,14] Briefly, a continuous molecular beam is crossed with a pulsed electron beam (100 ns) at right angles. The molecular beam is produced by a gas flow from a long needle with a diameter of 0.4 mm passing through a skimmer. The top of the needle is about 2 cm above the skimmer and the orifice of the skimmer is about 6 cm above the electron beam. The interaction volume is smaller than 4 mm×4 mm×4 mm. About 100 ns after the decay of the electron beam a pulsed voltage is applied to the extraction mesh of the mass spectrometer. The ions are extracted into a specially designed focusing time-of-flight (FTOF) mass spectrometer. The shield plates in the interaction region of the FTOF mass spectrometer make the extraction mesh perform as a plane-convex lens, which focuses the ions close to the axis of the FTOF mass spectrometer after the ions leave the ion source region. It also makes the divergence angle smaller than that in the extraction system of a normal Wiley-McLaren TOF mass spectrometer. The flight tube of the FTOF mass spectrometer is segmented into two tubes of identical length with a fine mesh in between. The fine mesh performs as a symmetrically spherical lens if the voltage applied to it is about 1.3–1.4 times higher than the voltage on the flight tubes. It makes the detection plane the image of the acceleration plane. In the experiments the voltage applied to the extraction mesh is typically −0.6 kV, that on the flight tubes is −1.27 kV, and that on the focusing mesh is −1.70 kV. Experimentally the complete collection of the ions is verified by deflecting the ion beam and counting the respective numbers of the fragments. If a flat top can be observed in the deflection curves, we conclude that all the ions have been collected by the detector, which is a microchannel plate (MCP) with a diameter of 37 mm (Hamamatsu 1208-3DS). The output of the microchannel plate is amplified by a fast preamplifier (SR 445) and discriminated by a constant fraction discriminator (TC454). The amplification of the microchannel plate

is dependent on the mass of the ions. The amplitude of the ion pulses decreases as the mass of the ions increases. The constant fraction discriminator gives a fast pulse ($\leqslant 4$ ns) with a constant amplitude if it obtains a pulse with an amplitude above the threshold of the discriminator. The threshold of the discriminator is adjusted to an amplitude where the ion signal is transmitted and the noise is eliminated. The output of the constant fraction discriminator is counted by a multichannel scaler (FAST 7886E).

As described in detail in a previous publication,[13] the focusing effect of the present time-of-flight mass spectrometer raises significantly the tolerance of the detection system to the initial kinetic energy and the starting position of the ions. Ion trajectory calculations show that the ions with an initial kinetic energy as high as 15 eV can be collected with the same efficiency as the thermal ions in the focusing time-of-flight mass spectrometer. The collection efficiency is only determined by the transmission of the meshes and the open area of the microchannel plate. The complete collection of the ions are further verified *experimentally* by observing the deflection curves. Since the fields inside the time-of-flight mass spectrometer are only electrostatic, the ion trajectories are thus mass independent. The ions are accelerated to 3.5 keV by the biased voltage of the MCP when they arrive at the MCP. The amplification of the MCP is in saturation so that it has the same detection efficiency to all the ions.[15] The counting electronics of the system is also mass independent. Hence we believe that the present system detects all the ions of different masses and different initial kinetic energies with equal efficiencies.

The time-of-flight mass spectra of the ionic fragments produced by electron impact direct and dissociative ionizations, are recorded by the multichannel scaler with a time resolution of 0.5 ns. The mass peaks are broadened by the initial kinetic energies of the fragments. Since all the ions with different initial kinetic energies are collected with the same efficiency, we can obtain the initial kinetic energy distributions of the ionic fragments by analyzing the time-of-flight profiles of the individual mass peaks. The method has been described in detail by Schäfer *et al.*[16] The resolution of the present kinetic energy analysis depends on the mass of the ions, which is about 0.2 eV at the mass of 30 amu. At lower masses the kinetic energy resolution is even lower. As a result, the subpeaks on the kinetic energy distributions are usually not real structures. As stated in a previous paper,[13] the error of the scale of the kinetic energy is about $\pm 20\%$.

The absolute cross sections of the molecules to be measured are obtained by normalizing the ion counts to those of a well-known gas like argon. Initially the ion counts of Ar^+ are recorded for electron energies at a particular backing pressure of argon. Then the ion counts of the fragments of ethane are recorded at the same backing pressure of ethane. All other experimental conditions are kept unchanged. The pressures of the gases in the small chamber above the needle are kept low enough so that the gas flow is in the effusive flow region. The absolute partial cross sections (e.g., C^+ from C_2H_6) are obtained by

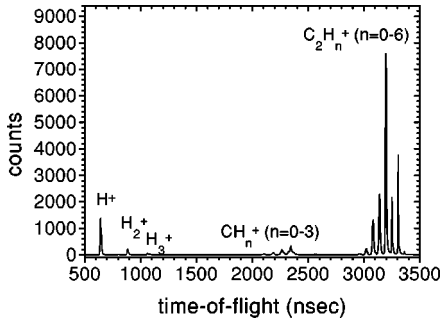

FIG. 1. Mass spectrum of C_2H_6 at an electron energy of 200 eV.

$$\sigma_{C^+} = \frac{I_{C^+}}{I_{Ar^+}} \sigma_{Ar^+}, \tag{1}$$

where I is the number of counts. Argon is used as the reference gas because its ionization cross section has been well established. In this work, the very recent result of Straub *et al.* has been taken as the reference value.[17] The errors in the cross sections of the fragment ions relative to the total values originate mainly from the data fluctuations, the gas pressure stability in the measurements, and the other isotopes of carbon. Usually we make at least 5 independent measurements and get the data fluctuations from these independent measurements. The counts from the background gas are measured without the molecular beam and are usually less than 5% of the total counts. They are subtracted. Unless otherwise stated, the error of the partial cross sections with respect to the total cross section is about 6%. The normalization of the data caused an error of 6%. The errors of the absolute cross sections are believed to be about 10%.

III. RESULTS AND DISCUSSION

A. Cross section measurements

A typical time-of-flight mass spectrum of ethane at an electron energy of 200 eV is shown in Fig. 1. The ionic fragments include $H_n^+(n=1-3)$, $CH_n^+(n=0-3)$, and $C_2H_n^+(n=0-6)$. We can see that most of the mass peaks are well resolved. The most abundant product is $C_2H_4^+$ instead of the parent ion $C_2H_6^+$. The mass peaks of CH_2^+ and CH_3^+ are broadened significantly by the initial kinetic energies of the two fragments. As a result the two mass peaks are not completely resolved at the bottom. The doubly charged fragments of $C_2H_5^{++}$ and $C_2H_3^{++}$ are also observed in the present work, but they cannot be resolved from CH_3^+ and CH_2^+, which will cause an additional error of 5% in the measurements of CH_3^+ and CH_2^+. The tail of the most abundant fragment, $C_2H_4^+$, slightly overlaps the mass peak of $C_2H_5^+$, which results in an additional error of about 2% for $C_2H_4^+$ and of about 5% for $C_2H_5^+$, respectively.

The ion counts as a function of the deflection voltages are shown in Fig. 2, separated in groups of $\Sigma C_2H_n^+(n=0-6)$, $\Sigma CH_n^+(n=0-3)$, H_3^+, H_2^+ and H^+. We see that all the groups show a constant number of counts for the X deflection voltage from -0.9 to -1.6 kV, and for the Y deflection voltage from -1.0 to -1.6 kV. In the measurement of the cross sections we set the X and Y deflection voltages at

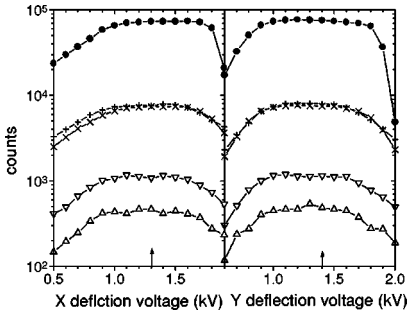

FIG. 2. The ion counts produced by the dissociative ionizations of C_2H_6 at an electron energy of 200 eV vs the X and Y deflection voltages. $(-\bullet-)$ $\Sigma C_2H_n^+(n=0-6)$; $(-\times-)$ $\Sigma CH_n^+(n=0-3)$; $(-\triangle-)$ H_3^+; $(-\triangledown-)$ H_2^+; $(-+-)$ H^+. All the voltages should be considered negative. The deflection voltage is fixed to the position indicated by the arrow when the voltage in the perpendicular direction is adjusted. For the cross section measurements the deflection voltages are fixed to both arrow positions.

-1.3 and -1.4 kV, respectively. We thus guaranteed experimentally that all the ions are collected to the detector with equal efficiencies, which is just determined by the transmission of the meshes and the physical area of the microchannel plate.

The cross section values for the electron energy from threshold to 600 eV are tabulated in Table I and are shown in Figs. 3–6, respectively. For comparison the existing data are also shown in the figures, which include the total cross section measurements of Catham *et al.*,[8] Durić *et al.*,[11] Nishimura and Tawara[12] as well as the partial cross section measurements of Catham *et al.*,[8] and Grill *et al.*[9] Catham *et al.* normalized their relative partial cross sections to their total cross section measurements. Grill *et al.* normalized their relative measurements to the total cross section data of Durić *et al.*[11] However, in both normalizations, the authors did not consider the contributions from the hydrogen fragments, $H_n^+(n=1-3)$. Whereas the present work shows that the contributions from the hydrogen fragments is about 10% of the total cross section. The present measurement gets a total cross section which is about 10% higher than the values of Catham *et al.* and Durić *et al.* at 100 eV. All the fragments are considered in the normalization, the data for the fragments of $C_2H_n^+(n=0-6)$ and $CH_n^+(n=0-3)$ can thus be compared directly with the results of Catham *et al.* and Grill *et al.*

The results for the electron impact direct and dissociative ionization of C_2H_6 into the ionic products of $C_2H_n^+$ $(n=0-6)$ are shown in Figs. 3(a)–3(f), respectively. The results of Catham *et al.*[8] and Grill *et al.*[9] are also included for comparison. Generally the present work agrees with the results of Catham *et al.* within the mutual experimental errors, whereas the present work gives a much smaller experimental error. The agreement between the present work with that of Grill *et al.* is not satisfactory. For direct ionization, the present results and those of Catham *et al.* agree within 5% in the peak region, but both results exceed those of Grill *et al.* by about 30%. For $C_2H_5^+$ our result agrees with that of Catham *et al.* within 5%, but exceeds that of Grill *et al.* by 20%. For the fragments of $C_2H_n^+(n=0-4)$, all the existing results tend to agree with our measurements within the mutual error limits. However, the agreement with respect to the relative shape is very poor. The results of Catham *et al.* are usually higher at high electron energies, whereas the results

TABLE I. The ionization cross sections (in unit of 10^{-16} cm^2) for electron impact on C_2H_6.

EE	H+	H_2^+	H_3^+	C^+	CH^+	CH_2^+	CH_3^+	C_2^+	C_2H^+	$C_2H_2^+$	$C_2H_3^+$	$C_2H_4^+$	$C_2H_5^+$	$C_2H_6^+$	total
600	0.141	0.024	0.011	0.007	0.011	0.041	0.099	0.007	0.032	0.217	0.385	1.20	0.293	0.366	2.84
550	0.155	0.027	0.012	0.009	0.013	0.045	0.107	0.008	0.035	0.234	0.411	1.28	0.313	0.391	3.04
500	0.168	0.030	0.013	0.009	0.015	0.049	0.117	0.009	0.039	0.248	0.434	1.34	0.331	0.410	3.21
450	0.187	0.033	0.014	0.011	0.017	0.054	0.127	0.010	0.043	0.267	0.464	1.41	0.347	0.427	3.42
400	0.215	0.038	0.016	0.013	0.020	0.063	0.141	0.012	0.050	0.296	0.505	1.53	0.375	0.465	3.75
350	0.239	0.041	0.017	0.014	0.024	0.071	0.157	0.013	0.056	0.326	0.538	1.61	0.391	0.487	3.99
300	0.283	0.049	0.020	0.017	0.030	0.083	0.180	0.017	0.065	0.367	0.598	1.76	0.424	0.534	4.43
275	0.307	0.053	0.022	0.018	0.032	0.088	0.192	0.019	0.073	0.382	0.623	1.82	0.442	0.548	4.63
250	0.339	0.057	0.024	0.020	0.037	0.096	0.206	0.020	0.078	0.414	0.655	1.92	0.462	0.576	4.91
225	0.371	0.065	0.027	0.023	0.041	0.105	0.225	0.023	0.090	0.445	0.698	2.01	0.480	0.606	5.22
200	0.400	0.071	0.029	0.025	0.044	0.112	0.238	0.026	0.097	0.477	0.728	2.08	0.503	0.629	5.47
175	0.440	0.076	0.031	0.027	0.048	0.125	0.258	0.028	0.107	0.509	0.770	2.15	0.517	0.650	5.75
150	0.470	0.082	0.034	0.029	0.055	0.136	0.277	0.030	0.118	0.548	0.813	2.24	0.533	0.676	6.06
125	0.495	0.090	0.036	0.031	0.063	0.149	0.298	0.032	0.132	0.597	0.861	2.34	0.560	0.709	6.40
100	0.495	0.098	0.038	0.030	0.067	0.160	0.319	0.032	0.143	0.655	0.923	2.49	0.583	0.744	6.79
90	0.473	0.096	0.038	0.029	0.066	0.161	0.320	0.029	0.142	0.667	0.936	2.52	0.593	0.746	6.83
80	0.418	0.089	0.040	0.024	0.061	0.153	0.317	0.026	0.140	0.664	0.937	2.51	0.583	0.750	6.72
70	0.363	0.086	0.035	0.021	0.056	0.151	0.300	0.022	0.135	0.673	0.954	2.54	0.592	0.754	6.70
60	0.288	0.068	0.033	0.017	0.045	0.139	0.272	0.017	0.122	0.666	0.956	2.61	0.593	0.768	6.61
50	0.190	0.048	0.020	0.010	0.032	0.102	0.216	0.010	0.098	0.633	0.904	2.51	0.570	0.730	6.09
45	0.160	0.034	0.014	0.004	0.023	0.080	0.175	0.005	0.076	0.589	0.891	2.51	0.573	0.739	5.89
40	0.117	0.025	0.007		0.010	0.066	0.144		0.051	0.526	0.840	2.52	0.581	0.764	5.68
35	0.068	0.015	0.002			0.038	0.109		0.022	0.399	0.716	2.36	0.558	0.687	5.07
30	0.039	0.007				0.019	0.091			0.310	0.532	2.11	0.507	0.664	4.47
25	0.009	0.002					0.070			0.225	0.362	1.43	0.346	0.475	3.13
20							0.032			0.080	0.135	0.49	0.122	0.168	1.12
17.5							0.019			0.044	0.065	0.25	0.058	0.080	0.56

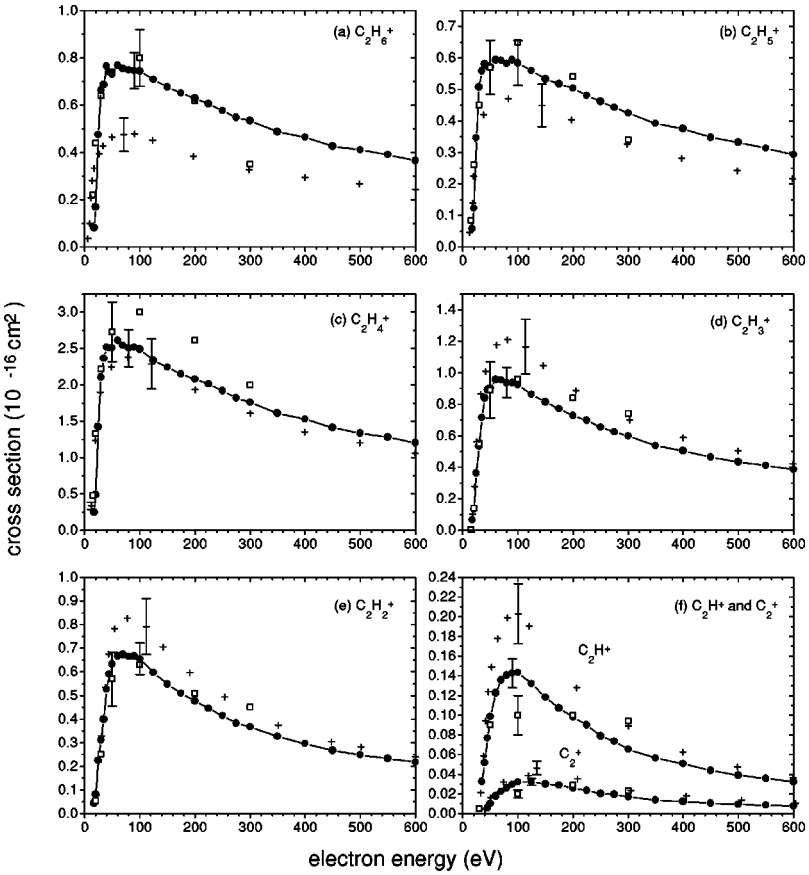

FIG. 3. Cross sections of the electron impact direct and dissociative ionizations of C_2H_6 into the fragments of $C_2H_n^+(n=0-6)$. (a) $C_2H_6^+$, (b) $C_2H_5^+$, (c) $C_2H_4^+$, (d) $C_2H_3^+$, (e) $C_2H_2^+$, (f) C_2H^+ and C_2^+. (−●−) The present work, (□) Catham *et al.* (Ref. 8), (+) Grill *et al.* (Ref. 9).

of Grill *et al.* are higher at low electron energies and lower at high electron energies.

The fragments of $CH_n^+(n=0-3)$ are more energetic than the group of $C_2H_n^+(n=0-6)$. For these fragments, the results of Catham *et al.* usually lie below the present values by a factor of 2–3 in the peak regions. The results of Grill *et al.* generally agree with the present work within the mutual error limits, but the relative shape of their results again deviates from the present measurements.

Catham *et al.* measured the partial cross sections with a calibrated quadrupole mass spectrometer. As concluded in a previous paper[13] the quadrupole mass spectrometer can give relatively accurate results only for those fragments which have similar kinetic energy distributions to the parent ion. The transmission of the quadrupole mass spectrometer is strongly dependent on the kinetic energy distributions of the ions. For the fast fragments the measurement with a quadrupole mass spectrometer usually gives a much lower value.

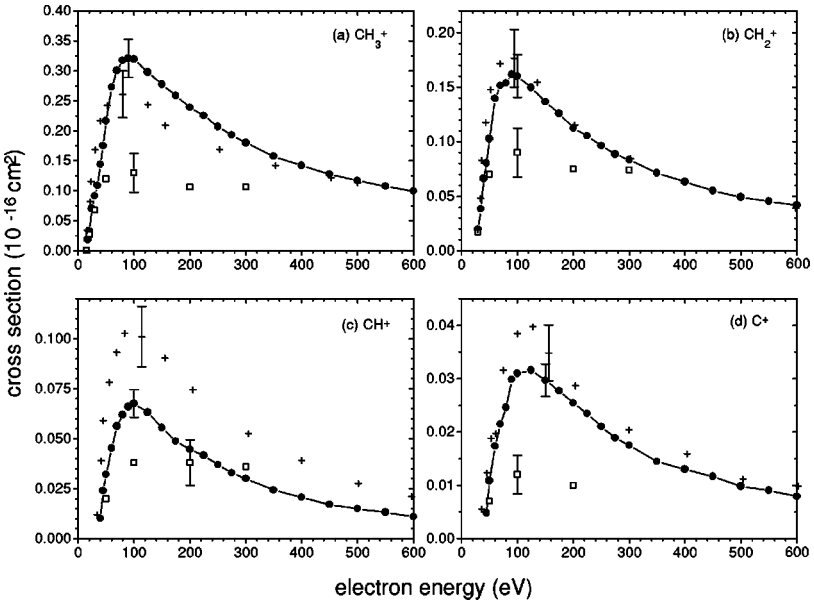

FIG. 4. Cross sections of the electron impact dissociative ionization of C_2H_6 into the fragments of $CH_n^+(n=0-3)$. (a) CH_3^+, (b) CH_2^+, (c) CH^+, (d) C^+. (−●−) The present work, (□) Catham *et al.* (Ref. 8), (+) Grill *et al.* (Ref. 9).

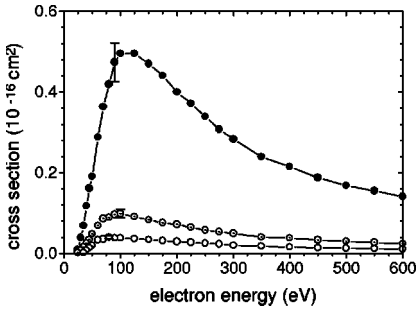

FIG. 5. Cross sections of the electron impact dissociative ionization of C_2H_6 into the fragments of $H_n^+(n=1-3)$. $(-\bullet-)$ H^+, $(-\odot-)$ H_2^+, $(-\bigcirc-)$ H_3^+. No previous results exist.

We can therefore explain why the results of Catham *et al.* generally agree with the present work for the fragments of $C_2H_n^+(n=0-6)$, and lie much lower than the present results for the light fragments such as $CH_n^+(n=0-3)$. The experimental setup of Grill *et al.* strongly discriminates against fast fragments, the collection efficiency decreases by at least 2 orders of magnitude for the ions with a kinetic energy from thermal to 10 eV. In order to achieve a relatively accurate value for the fast fragments, the authors separated the ions into different groups according to their kinetic energies. The relative abundance of the different groups was determined by measuring the kinetic energy distributions of the fragments. They corrected the collection efficiency of different groups with the calculated collection efficiencies. The collection efficiencies were calculated theoretically, which usually just considers an ideal experiment. This may cause unpredictable errors to their final cross section values. Furthermore, the relative abundance of the different groups depends on the electron energy. If one wants to perform such a calibration, one has to do it for every electron energy. This is not the case in the work of Grill *et al.* It makes the measurements of the relative shape of the cross sections inaccurate. Usually at higher electron energies the abundance of the fast ions is higher. Grill *et al.* made the calibration at an electron energy of 100 eV. In this manner they underestimated the abundance of the fast ions at higher electron energies and reported a relatively low value. The present work measures all the fragments directly. No calibration other than the normalization is required. So we believe that the present results are more reliable with respect to the relative shape as well as the absolute values.

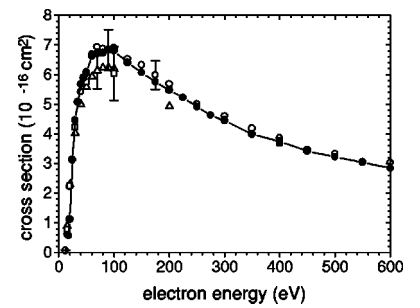

FIG. 6. Total cross sections of the electron impact ionization of C_2H_6. $(-\bullet-)$ The present work, (□) Catham *et al.* (Ref. 8), (△) Durić *et al.* (Ref. 11), (○) Nishimura and Tawara (Ref. 12).

The cross sections for the hydrogen fragments are shown in Fig. 5. No previous results exist for comparison. We see that the total value for the hydrogen fragments exceeds even that of the fragments of $CH_n^+(n=0-3)$. However, they were not considered before.

The fragments of $C_2H_5^{++}$ and $C_2H_3^{++}$ are also observed in the present measurements. However, they cannot be resolved from the energy-broadened long tails of the mass peaks of CH_3^+ and CH_2^+. We estimate that the cross section for $C_2H_5^+$ is smaller than 1×10^{-18} cm^2 at an electron energy of 200 eV. That for $C_2H_3^+$ is even smaller. The other isotopes may cause some errors in the measurements. Generally the error caused by the other isotopes of carbon is about 2%. For $C_2H_5^+$ the cross section value might be overestimated by 5%.

The total cross sections are shown in Fig. 6 together with the measurements of Catham *et al.*,[8] Durić *et al.*[11] and Nishimura and Tawara.[12] The present results are about 2% lower than the results of Nishimura and Tawara at 100 eV. The two sets of data also show excellent agreement in the relative shape. The results of Durić *et al.*[11] lie below the present values by about 10% and also agree with the present work with respect to the relative shape. The data of Catham *et al.*[8] showed a different relative shape. All the data agree with each other within the mutual error limits.

B. Appearance potentials

The appearance potentials of the ionic products were measured with an accuracy of ±1 eV, as listed in Table II. The values in the third column are the calculated results from the heat of formation of each fragment. The data for the heat of formation are from Lias *et al.*[18] In the calculation we assumed that all the fragments are produced in the electronic and vibrational ground states. The other existing experimental values are also included. Compared with the experimental results and the calculation, we see that only the experimental results for the ionic products such as $C_2H_6^+$, $C_2H_5^+$, $C_2H_4^+$, $C_2H_3^+$, $C_2H_2^+$, CH_3^+ and H_2^+ agree with the calculation. For the other products the experimental results do not agree with the calculation. For the fragments of $C_2H_6^+$, $C_2H_5^+$, $C_2H_4^+$, $C_2H_3^+$, $C_2H_2^+$ and CH_3^+, a variety of measurements exists. Generally they agree with each other within the experimental uncertainties. The only previous complete set of data are from Au *et al.*[6] Comparing their results with the present work, the appearance potentials agree with each other for the fragments other than C_2^+, C^+ and H_2^+. The appearance potentials for C_2^+, C^+ and H_2^+ in the present work are 34.0, 32.0, and 18.0 eV, respectively. They are below the results of Au *et al.* by 6.0, 11.0, and 11.5 eV, respectively. The discrepancy might be due to two reasons. One is that the sensitivity of the experiment of Au *et al.* is not high enough, but this is quite unlikely since Au *et al.* can also collect all the products without discrimination. The other is that, although in both experiments ethane is excited by electron impact, Au *et al.* measure the electron energy-loss $(e,\ e+\text{ion})$ coincidence spectra, which actually just detects the dipole-allowed transitions. In the electron impact excitation also dipole-

TABLE II. The appearance potentials (in electronvolt) of different fragment in the dissociative ionization of C_2H_6.

ion	this work	Cal. (other products)	Ref. 6	Ref. 19	Ref. 20	Ref. 21	Ref. 22	Ref. 23	Ref. 24
$C_2H_6^+$	11.5	11.52	11.0	11.5	11.50	11.5	11.6	11.6	11.66
$C_2H_5^+$	12.8	12.49 (H)	12.0	12.3	12.00	12.8	12.8	12.2	12.66
$C_2H_4^+$	12.7	11.93 (H_2)	11.0	11.9	12.08	12.0		12.1	12.24
$C_2H_3^+$	15.4	14.67 (H_2+H)	13.5	14.4					15.22
$C_2H_2^+$	15.3	14.65 ($2H_2$)	14.0	14.5					15.35
C_2H^+	28.8	20.70 ($2H_2$+H)	27.0						
C_2^+	34.0	21.50 ($3H_2$)	40.0						
CH_3^+	14.0	13.72 (CH_3)	14.0	14.7		14.0	13.6		13.46
CH_2^+	25.8	19.00 (CH_3+H)	25.0						
CH^+	30.0	19.21 (CH_3+H_2)	31.0						
C^+	32.0	18.90 (CH_3+H_2+H)	43.0						
H_3^+	33.2	15.10 (C_2H_3)	33.0						
H_2^+	18.0	16.85 (C_2H_4)	29.5						
H^+	20.5	18.39 (C_2H_4+H)	20.5						

forbidden transitions can occur. Electron impact can thus excite ethane to some ionized states via quadrupole- or higher order- allowed transitions and produce these ionic fragments. This is particularly true at the electron energies near threshold.[25,26] This electron impact dipole-forbidden transition was also observed in the electron energy-loss spectroscopy of the Rydberg states of C_2H_4 and C_2D_4.[27]

C. Kinetic energy release and dissociation pathways

1. Channels to $C_2H_n^+(n=0-6)$

From Table II we see that the appearance potentials of the ionic products $C_2H_n^+(n=2-6)$ agree with the calculations from the heat of formation within the experimental uncertainties. Since the other dissociation limits, which correspond to different combinations of neutral products or the same neutral products in different electronic states, considerably exceed the calculated values shown in Table II, the starting channels of the dissociative ionizations of $C_2H_6^+$ into different ionic fragments are believed to be

$$C_2H_6^+ \rightarrow C_2H_5^+ + H(1s), 12.55 \text{ eV}, \quad (2)$$

$$C_2H_6^+ \rightarrow C_2H_4^+ + H_2(X\Sigma_g^+), 11.87 \text{ eV}, \quad (3)$$

$$C_2H_6^+ \rightarrow C_2H_3^+ + H_2(X\Sigma_g^+) + H(1s), 14.80 \text{ eV}, \quad (4)$$

$$C_2H_6^+ \rightarrow C_2H_2^+ + 2H_2(X\Sigma_g^+), 14.64 \text{ eV}, \quad (5)$$

where all the ions of $C_2H_n^+(n=2-6)$ are also in the electronic ground states. The energies which follow the reaction channels in Eqs. (2)–(5) are the corresponding dissociation limits. The kinetic energy distributions of the ions at the electron energy of 28 eV are shown in Fig. 7. Among all the ions only the kinetic energy distribution of $C_2H_6^+$ shows a maximum at 0 eV with a tail extending to about 0.3 eV. This distribution shows the resolution of the kinetic energy measurements in the present work for the ions of $C_2H_n^+(n=2-6)$. The resolution is about 0.2 eV. All the other ions of $C_2H_n^+(n=2-5)$ show a maximum at different kinetic energies above 0 eV, which suggests that the electronic states of $C_2H_6^+$ which correspond to the dissociation channels to the above ionic fragments, are dominated by repulsive states. Figure 7 also shows that very few $C_2H_4^+$ ions are located at 0 eV, whereas there is a high peak around 0.1 eV, suggesting that most of the electronic states of $C_2H_6^+$ which correspond to the dissociation limit of $C_2H_4^+ + (H,H_2)$ are repulsive levels. The measurements of the appearance potentials of the fast ions show that these repulsive levels are located at about 13.5 eV above the ground state of molecular ethane in the Franck-Condon region.

Molecular orbital calculations predicted that the ground state electronic configuration for ethane should be

$$(1a_{1g})^2(1a_{1u})^2(2a_{1g})^2(2a_{1u})^2(1e_u)^4(3a_{1g})^2(1e_g)^4\ {}^1A_{1g}\ .$$

Photoelectron and $(e,2e)$ spectroscopy showed[1,4] that as the energy of the incident electrons increases to threshold (11.5 eV), the first electron to be ejected out of the molecule will be a $1e_g$ electron. The $1e_g$ orbit is C-H bonding and C-C antibonding. The ejection of the $1e_g$ electron results in a series of bound states, which might be the origin for the formation of stable $C_2H_6^+$. $C_2H_6^+$ is expected in the C_{2h} structure with a ''normal'' C-C bond length.[2] If the energy of the incident electrons is increased further to about 13 eV, a $3a_{1g}$ or $1e_u$ electron can be ejected. The $3a_{1g}$ orbit is strongly C-C and C-H bonding. The $1e_u$ orbit is also C-C and C-H bonding. The electronic states of the ethane cation resulting from the removal of these electrons are thus very unstable and subject to dissociation. This was the reason why

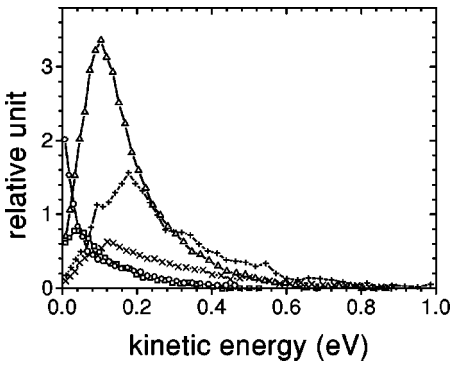

FIG. 7. The kinetic energy distributions of the ionic products $C_2H_n^+(n=2-6)$ at the electron energy of 28 eV. $(-\bigcirc-)$ $C_2H_6^+$, $(-\square-)$ $C_2H_5^+$, $(-\triangle-)$ $C_2H_4^+$, $(-\times-)$ $C_2H_3^+$, and $(-+-)$ $C_2H_2^+ \times 5$.

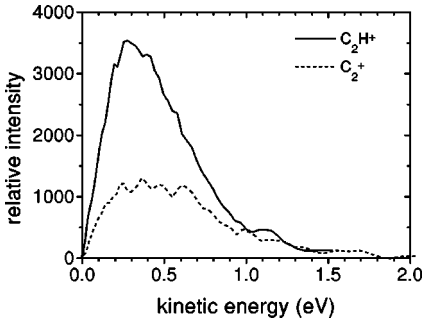

FIG. 8. The kinetic energy distributions of C_2H^+ and C_2^+ at the electron energy of 50 eV.

Rabalais and Katrib observed a diffuse spectrum in their photoelectron work.[1] These levels are dissociative. This is also the reason why we always observed that the fragments are mostly distributed in the higher kinetic energy regions. At even higher electron energies the electron in the molecular orbitals $2a_{2u}$ and $2a_{1g}$ can be ejected and some stable ethane cation can also be formed, but the oscillator strengths of the transitions are much smaller than for those mentioned above.

The above analysis can also be used to explain qualitatively why the abundance of the parent ions does not exceed that of some ionic fragments, whereas it usually does in small molecules.[13,14] Since most of the electronic states of $C_2H_6^+$ are repulsive, C_2H_6 tends to dissociate after it is ionized. Since the dissociation limit of $C_2H_4^+ + H_2(X\ \Sigma_g^+)$ is the lowest among all the channels, the potential surface is the steepest in the coordinate of $C_2H_4^+ + H_2(X\ \Sigma_g^+)$. The abundance of $C_2H_4^+$ thus exceeds all the other ionic products.

The kinetic energy distributions of C_2H^+ and C_2^+ at the electron energy of 50 eV are shown in Fig. 8. For C_2H^+ and C_2^+ the appearance potentials are above the calculated threshold. The ions are distributed in a similar profile at the electron energies close to threshold, suggesting that the shape of the potential surfaces are repulsive. The processes involved in many-body processes and their detailed analysis requires the coincidence measurement of the products, and the determination of the final states of the fragments. Those are beyond the scope of the present paper.

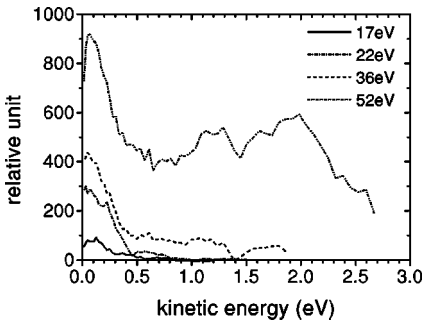

FIG. 9. The kinetic energy distributions of CH_3^+ at the electron energies of 17, 22, 36, and 52 eV.

2. Channels to $CH_n^+ (n=0-3)$

The kinetic energy distributions of CH_3^+ at the electron energies of 17, 22, 36, and 52 eV are shown in Fig. 9. Experiments show that for the electron energies from threshold to 28 eV, the relative kinetic energy distributions of CH_3^+ are almost identical, with a peak around 0.2 eV. All the ions are distributed at the kinetic energy below 0.5 eV. At the electron energy of 32 ± 2 eV fast CH_3^+ ions appear with a kinetic energy between 0.5 and 2.5 eV. At higher electron energies the ions consist mainly of two parts. One is due to the slow ions which appear at low electron energies, whereas the other is due to the fast ions which appear at 32 ± 2 eV. The ratio of the fast to the slow ions increases even further at higher electron energies.

The kinetic energy distribution can be explained by noting the molecular orbits and the double ionization. The appearance potential of CH_3^+ is consistent with the heat of formation calculations. The starting channels for the formation of CH_3^+ are expected to be

$$C_2H_6^+ \rightarrow CH_3^+ + CH_3. \tag{6}$$

The calculated threshold is 13.72 eV. The experiment shows that it is 14 ± 1 eV. At this electron energy the molecules are expected to be ionized preferably to the $3a_{1g}^{-1}$ or $1e_u^{-1}$ orbits. Since both the $3a_{1g}$ or $1e_u$ electrons in the ethane molecule are C-C bonding, the electronic states of the ethane cation in the $3a_{1g}^{-1}$ or $1e_u^{-1}$ orbits are thus dissociative. These states are the origin for the CH_3^+ ions at low kinetic energies. At the electron energy above 30 eV, CH_3^+ can be produced by the double ionization of the ethane molecules, i.e.,

$$C_2H_6^{++} \rightarrow CH_3^+ + CH_3^+. \tag{7}$$

The heat of formation calculations show that the threshold for this process is 23.55 eV. The electronic states of $C_2H_6^{++}$ should be Coulomb repulsive. The appearance potential of the fast ions indicates that the potential surface of the ground state of the doubly ionized ethane in the Franck-Condon region is located at about 32 ± 2 eV. Compared with the dissociation limit of 23.55 eV, the excess energy is about 8.5 ±2 eV. This excess energy is shared by the two CH_3^+ ions. The kinetic energy measurements show that it is very probable that some part of the excess energy is transferred into the vibrational excitation of the ions since this dissociation channel is also associated with severe geometric distortion of the molecule.

The production of CH_2^+ ions is also involved in the ejection of an electron in the C-C bonding orbital, which makes the potential energy surface repulsive. The starting channel is possibly the reaction

$$C_2H_6^+ \rightarrow CH_2^+ + CH_3 + H, \tag{8}$$

and the calculated dissociation limit is 19.0 eV. The measured appearance potential is 25.8 eV where the excess energy is shared by the fragments in a complicated way. The measured kinetic energy distributions of CH_2^+ at the electron energy of 36, 44, and 100 eV are shown in Fig. 10. At the electron energy close to threshold fast ions are also observed, suggesting that the potential energy surface is located above the dissociation limit and is repulsive. At the electron energy

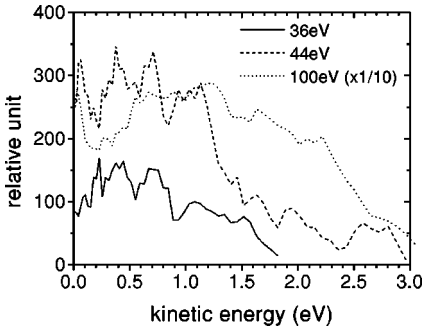

FIG. 10. The kinetic energy distributions of CH_2^+ at the electron energies of 36, 44, and 100 eV.

of 40 ± 2 eV a tail appears at the kinetic energy above 2 eV. This tail might be from the dissociation of doubly ionized molecules in the channels of either

$$C_2H_6^{++} \rightarrow CH_2^+ + CH_3^+ + H, \tag{9}$$

or

$$C_2H_6^{++} \rightarrow 2CH_2^+ + H_2. \tag{10}$$

The heat of formation calculations show that the thresholds for these processes are 28.84 and 28.55 eV, respectively. We cannot distinguish these two processes. In either process the excess energy is 11 ± 2 eV. It is reasonable that CH_2^+ gets a kinetic energy higher than 2 eV.

The kinetic energy distributions of CH^+ and C^+ at the electron energy of 50 eV are shown in Fig. 11. At even higher electron energies we did not observe the subpeak around 2.5 eV measured by Fuchs and Taubert.[28] Comparing the work of Fuchs and Taubert with that of Locht *et al.*,[29] it is very probable that the measurement of Fuchs and Taubert underestimated slow ions and overestimated fast ions. If these fast ions exist they might also be from the dissociation of doubly ionized molecules.

3. Channels to H_n^+

The present work has low kinetic energy resolution with respect to the ions of $H_n^+(n=1-3)$ since the mass peaks become much narrower for these ions. We did not observe the structures measured by Fuchs and Taubert.[28] We can see that most H_3^+ are distributed at high energies. The present work gets a much lower appearance potential for H_2^+ than Au *et al.*,[6] which is close to the threshold calculated from the heat of formation. This suggests that the starting pathway for the production of H_2^+ is

$$C_2H_6^+ \rightarrow H_2^+ + C_2H_4. \tag{11}$$

Au *et al.* observed a much higher appearance potential for H_2^+ in their dipole measurement. It is very unlikely that this was caused by the sensitivity of their measurements. We assign the excitation close to threshold to dipole-forbidden transitions.

The kinetic energy resolution for H^+ is about 1.5 eV. The appearance potential measurements suggest that the starting channel is

$$C_2H_6^+ \rightarrow H^+ + C_2H_4 + H. \tag{12}$$

Our measurements show that most H^+ are distributed around 1 eV. The kinetic energy resolution of the present measurements for H^+ is insufficient to allow a further analysis.

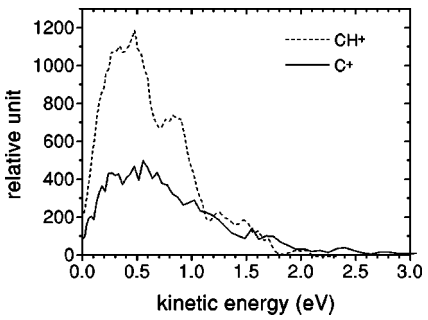

FIG. 11. The kinetic energy distributions of CH^+ and C^+ at the electron energy of 50 eV.

IV. CONCLUSIONS

The cross sections for a complete set of singly charged fragments of the electron impact ionization as well as dissociative ionization of ethane have been measured for electron energies from threshold to 600 eV. The previous partial cross section measurements suffered from either the loss of fast ions or indirect calibration. In some cases those results show very poor agreement with the present work in either the relative shape or the absolute values. The present work demonstrates the complete collection of all the ionic products directly in the experiment. The results are thus believed to be reliable. The results of the products of $H_n^+(n=1-3)$ are obtained for the first time. The total cross section shows an excellent agreement with the previous measurements in both the relative shape and the absolute value. The appearance potentials of the ionic products are also measured. For most ionic fragments the present work agrees with that of Au *et al.*[6] except for the ions C_2^+, C^+ and H_2^+. The disagreement for these ions is explained by the dipole-forbidden transitions in the electron impact excitation process. The kinetic energy distributions of the ionic products are also measured. From the appearance potentials of the ionic products, the kinetic energy distributions, and the ejection of the electrons out of the different orbitals of the ethane molecule, we derived the starting channels for the ionic products.

ACKNOWLEDGMENTS

One of the authors (C.T.) is grateful to the Alexander von Humboldt Foundation for the financial support for staying at the Max-Planck-Institute for extraterrestrial Physics. The technical support of B. Steffes and the stimulating discussions with T. Sykora are also appreciated. Fruitful discussions with Dr. S. Schlemmer, who is with the Technical University of Chemnitz-Zwickau, Germany, are gratefully acknowledged.

[1] J. W. Rabalais and A. Katrib, Mol. Phys. **27**, 923 (1974).
[2] M. Huang and S. Lunell, Chem. Phys. **147**, 85 (1990).
[3] C. E. Hudson, D. J. McAdoo, and C. S. Giam, J. Comput. Chem. **17**, 1532 (1996).

[4] S. Dey, A. J. Dixon, I. E. McCarthy, and E. Weigold, J. Electron Spectrosc. Relat. Phenom. **9**, 397 (1976).
[5] J. H. M. Beijersbergen, W. J. van der Zande, P. G. Kistemaker, and J. Los, J. Phys. Chem. **97**, 11180 (1993).
[6] J. W. Au, G. Cooper, and C. E. Brion, Chem. Phys. **173**, 241 (1993).
[7] K. Kameta, S. Machida, M. Kitajima, M. Ukai, N. Kouchi, Y. Hatano, and K. Ito, J. Electron Spectrosc. Relat. Phenom. **79**, 391 (1996).
[8] H. Catham, D. Hills, R. Robertson, and A. Gallagher, J. Chem. Phys. **81**, 1770 (1984).
[9] V. Grill, G. Walder, P. Scheier, M. Kurde, and T. D. Märk, Int. J. Mass Spectrom. Ion Processes **129**, 31 (1993).
[10] B. L. Schram, M. J. van der Wiel, F. J. de Heer, and H. R. Moustafa, J. Chem. Phys. **44**, 49 (1966).
[11] N. Durić, I. Čadež, and M. Kurepa, Int. J. Mass Spectrom. Ion Processes **108**, R1 (1991).
[12] H. Nishimura and H. Tawara, J. Phys. B **27**, 2063 (1994).
[13] Cechan Tian and C. R. Vidal, J. Chem. Phys. **108**, 927 (1998).
[14] Cechan Tian and C. R. Vidal, J. Phys. B **31**, 895 (1998).
[15] B. Brehm, J. Grosser, T. Ruscheinski, and M. Zimmer, Meas. Sci. Technol. **6**, 953 (1995).
[16] K. Schäfer, W. Y. Baek, K. Föster, D. Gassen, and W. Neuwirth, Z. Phys. D **21**, 137 (1991).
[17] H. C. Straub, P. Renault, B. G. Lindsay, K. A. Smith, and R. F. Stebbings, Phys. Rev. A **52**, 1115 (1995).
[18] J. G. Lias, J. E. Bartmess, J. F. Liebman, J. L Holmes, R. D. Levin and W. G. Mallard, J. Phys. Chem. Ref. Data Suppl. 1 **17**, 1 (1988).
[19] R. L. Schoen, J. Chem. Phys. **37**, 2032 (1962).
[20] C. Backx, R. R. Tol, G. R. Wight, and M. J. van der Wiel, J. Phys. B **8**, 3007 (1975).
[21] J. W. Gallangher, C. E. Brion, J. A. R. Samson, and P. W. Langhoff, J. Phys. Chem. Ref. Data **17**, 9 (1988).
[22] B. Steiner, C. F. Giese, and M. G. Inghram, J. Chem. Phys. **34**, 189 (1961).
[23] J. A. Beran, A. K. Dhingra, W. Liu, and D. F. Mullica, Can. J. Chem. **53**, 1616 (1975).
[24] S. Tsuda and W. H. Hamill, J. Chem. Phys. **41**, 2713 (1964).
[25] S. P. Hernandez, P. J. Dagdigian, and J. P. Doering, J. Chem. Phys. **77**, 6021 (1982).
[26] I. Tokue, M. Kobyyashi, and Y. Ito, J. Chem. Phys. **96**, 7458 (1992).
[27] D. G. Wilden and J. Comer, J. Phys. B **13**, 1009 (1980).
[28] Von R. Fuchs and R. Taubert, Z. Naturforsch. A **19**, 1464 (1964).
[29] R. Locht, J. L. Olivier, and J. Momigny, Chem. Phys. **43**, 425 (1979).